International Journal of Ecosystems and Ecology Science (IJEES) **Vol. 13 (3):** 63-74 (2023)
https://doi.org/10.31407/ijees https://doi.org/10.31407/ijees13.3

THE HIGH-EFFICIENCY CR(VI) ADSORPTION USING POPLAR WOOD BASED ACTIVATED CARBON

Izge Demir[1], Aykut Caglar[2*], Derya Yildiz[1+]

[1+]Department of Chemical Engineering, Faculty of Engineering and Architecture, Eskisehir Osmangazi University, Eskişehir, 26040, Turkey;
[2]Department of Chemistry, Faculty of Sciences and Arts, Eskisehir Osmangazi University, Eskişehir, 26040 Turkey;*

[*] Corresponding Author Aykut Caglar and Derya Yildiz[+], e-mail: aykut_802@hotmail.com; aykut18.05.2015@gmail.com; dozcan@ogu.edu.tr;

Received July 2023; Accepted August 2023; Published September 2023;

DOI: https://doi.org/10.31407/ijees13.310

ABSTRACT

Activated carbons were obtained from poplar sawdust with H_3PO_4 activation in this study. Activated carbons were produced as 2:1 (PL2-400), 3:1 (PL3-400), and 4:1 (PL4-400) by mass chemical substance/chip ratio at 400 °C carbonization temperature with an impregnation process. These activated carbons' surfaces were identified by BET, SEM-EDX, and FTIR analyses. Cr(VI) heavy metal adsorption was carried with activated carbon (PL4-400, 1345.26 m^2/g), which has the highest surface area. Adsorption was carried out at the 2-9 pH range, in the range of 0.001-0.1 g activated carbon, and at temperatures of 25, 35, and 45 °C. The Kinetics of Cr(VI) adsorption was characterized by using adsorption kinetic models. The relationship between adsorbent and adsorbed is explained by Langmuir and Freundlich isotherm models. It was observed that the Cr(VI) adsorption on PL4-400 was more compatible with the Langmuir adsorption model. In addition, $\Delta G°$, $\Delta S°$, and $\Delta H°$ values were determined by making thermodynamic calculations, and the applicability of the adsorption was identified as endothermic and spontaneous.

Keywords: Waste water, Activated carbon, Cr(VI) adsorption,

INTRODUCTION

Although the rapidly increasing demand for the industry and its growth lead to economic growth, heavy metal pollution, which causes water and soil pollution, is greatly increasing. For a healthy life, small amounts of heavy metals such as iron, zinc, copper, and manganese are nutritionally essential. However, even at low concentrations some heavy metal ions can be reason serious environmental problems and vary diseases. Heavy metals are easily transferred to the food chain due to their high solubility in water and thus pose a serious threat to living things. Thus, it is required to develop effective materials and separation methods for the removal of these heavy metals [1-3].
Heavy metals such as Hg, Cd, Cu, Pb, Zn, As, and Cr are highly toxic and widely used by industries [4, 5]. Although trace amounts of these metals are required for metabolic activities to prevent disease in humans, their excessive concentrations can cause some health issues such as muscle diseases, cancer and Alzheimer's [6]. Cr(VI), which is reduced to Cr(III) by interacting in the human body such as nuclear enzymes, proteins, and nucleotides, is toxic and

carcinogenic even in small amounts. Exposure to large amounts of Cr ions can cause kidney, liver, and stomach disorders and even death [7-9]. Therefore, it is very important to remove Cr(VI) so that it does not harm nature and living things. It is generally used by methods such as chemical reduction, coagulation, biological treatment, and adsorption to remove chromium ions from water [10]. Of these methods, adsorption process is the preferred method because of its low energy consumption, environmental friendliness, and easy working conditions such advantages. Another advantage that highlights the adsorption process is that the adsorbent utilized to remove metal ions from the water has a loading capacity and high tendency [11, 12]. In the literature to remove heavy metal ions various materials such as Bentonite-Fe_3O_4 [5], Fe_3O_4-CS@BT [13], carbon nanotube [14], zeolites [15], cellulose nanofibers [16], and activated carbon [17, 18] were used as adsorbents. Among these materials, activated carbon is a valuable adsorbent to remove the heavy metals thanks to its high surface area and pore volume [19]. Although many carbon-containing materials are used to obtain activated carbon, coal is widely used to manufacture commercial activated carbon owing to its ideal adsorption efficiency. However, since commercial activated carbon from coal requires high investment costs for large-scale applications, it is of great interest to meet the manufacture of activated carbon from agricultural waste and industrial waste [20, 21]. There are many studies on different applications of activated carbon obtained from industrial and agricultural wastes in literature. It has been determined that hazelnut bagasse activated carbon is promising in the methanolysis and electrooxidation of NaBH4 as a metal-free catalyst through its high surface area and surface charge due to some bound ions [22]. Ghorbani et al [23]. reported that they obtained sugar beet bagasse based activated carbon and they used it for adsorption of Cr(VI). They emphasized that the activated carbon they obtained is environmentally friendly and low-cost, and it is also an effectual adsorbent for heavy metal adsorption from waste water.

The studies on the adsorption of Cr(VI) on to activated carbons are limited in the literature. Therefore, activated carbon, which is environmentally friendly, cheap, and obtained from waste, has great importance in heavy metal removal. Herein, the activated carbon from poplar sawdust (PL) was produced by the chemical activation method. BET, SEM-EDX, and FTIR analyses were used to characterize the activated carbons. The pH, adsorbent amount, contact time, and temperature effects on Cr(VI) adsorption with activated carbon were examined.

Experimental

1. Material and production of activated carbon

For adsorption processes, Cr(VI) stock solution was prepared with $K_2Cr_2O_7$ (Sigma-Aldrich). Then the stock solution was diluted and solutions were prepared at required concentrations. For Cr(VI) determination, 1,5 diphenylcarbazide (Merck), acetone (Sigma-Aldrich), and 0.2 N H_2SO_4 solution were used. In order to adjust the pH values of the solutions containing Cr(VI) 0.1 M HCl and NaOH were used.

The activated carbon was produced from poplar wood sawdust used for the Cr(VI) adsroption. First, the sawdust was sieved and divided into 0.224-0.425, 0.425-0.6, 0.6-.85, 0.85-1.0, and 1.0-1.8 mm particle sizes. $0.6<Dp<0.85$ mm particle size sample was dried at room conditions and stored in closed containers for use in the experiments. The sample was activated by the chemical activation method using an H_3PO_4 chemical agent. For the impregnation process, the chemical agent/wood sawdust ratio by mass was determined as 2:1, 3:1, and 4:1. The obtained carbons were named PL2-400, PL3-400, and PL4-400.

2. Characterization

The characteristics of activated carbon surface were identified as described in [24]. Activated carbon surface area was measured at 77 K by N_2 adsorption. The nitrogen isotherm was measured in approximately 10^{-5}-1 relative pressure (P/P_0) range. FTIR analysis was carried out to identify the functional groups of sawdust and activated carbon. SEM-EDX analysis was performed to image the surface microstructure.

3. Adsorption

1000 ppm stock solution of Cr(VI) was prepared from $K_2Cr_2O_7$ salt. Solutions of different concentrations used in adsorption studies were prepared by diluting the stock solution. The activated carbon was produced by H_3PO_4 activation wtih different impregnation ratios. The activated carbon which has a highest specific surface area was chosen as an adsorbent to remove the Cr(VI).

In order to examine the pH effect, 0.05 g adsorbent was added to the 50 mg/L solution and the experiments were performed at pH 2-9 range at 25 °C for 24 h. The pH values of the samples were readjusted with 0.1 N NaOH and 0.1 N HCl solutions. The adsorbent dose effect examined at an 50 mg/L initial concentration and pH=2 by added the activated carbon ranging from 0.001 g to 0.1 g. The experiments were performed for 24 h at 25 °C. To determine the

equilibration time, 0.05 g of activated carbon was added 50 mg/L solution at pH=2 and 25 °C. Samples were taken between 0-20 h and absorbance values were read in a UV spectrometer. In order to shorten the equilibrium time, the experiments were repeated with 0.1 g activated carbon for 50 mg/L solition at pH=2 and 25 °C. It was observed that equilibrium was reached in a shorter time by taking samples in the range of 0-8 h. For this reason, experimental studies were continued with 0.1 g activated carbon. To examine the temperature effect, experiments were performed with 50 mL solution at pH=2, initial concentration range of 50-250 mg/L and at 25 °C, 35 °C and 45 °C temperatures for 4 h. All adsorption experiments were performed for 50 mL solution.
Solutions of 1,5 diphenyl carbazide and 0.2 N H_2SO_4 were prepared for Cr(VI) determination in a UV spectrophotometer. These solutions were used to identify the amount of chrome present in the samples taken from the clear parts of the solutions after the adsorption process. For each sample, a certain amount of sample, 0.2 N H_2SO_4 and 1.5 diphenylcarbazide solution were added to 100 ml balloon jugs, respectively. Then, the solutions were stirred for 20 minutes, and then the absorbance values were read in a UV spectrophotometer to identify the amount of Cr(VI) remaining in the solutions. With these data, the remaining amount of Cr(VI) that unadsorbed in solution (Ce), the Cr(VI) amount that adsorbed on to carbon (qe), and the removal (%) values were calculated from Equation (1) and Equation (2), respectively. The obtained data were plotted and the the parameter effects on adsorption was determined.

$$qe = \frac{(C_o - C_e).V}{m} \quad (1)$$

where; C_0 is the primary concentration (mg/L), V is the volume of used solution (ml), m is the activated carbon mass (g).

$$Removal\ (\%) = \frac{(C_o - C_e)}{C_o}.100 \quad (2)$$

4. Kinetics

The 1st order and 2nd order models and diffusion model applying to determined the Cr(VI) adsorption kinetics. The pseudo-1st-order kinetic model is given as follows:

$$log(q_e - q_t) = log(q_e) - \frac{k_1 t}{2.303} \quad (3)$$

where; qt (mg/g) is the Cr(VI) amount that adsorbed per amount of carbon, k_1 (h^{-1}) is the pseudo-1st-order rate constant, t (h) is the contact time. The k_1 is obtained from the slope of the log(qe-qt) versus t graph. This model is described for the first moments of adsorption.
The pseudo-second-order model is given by Equation (4),

$$\frac{t}{q_t} = \frac{1}{k_2 q_e^{\,2}} + \frac{1}{q_e} t \quad (4)$$

where; qt is the Cr(VI) amount that adsorbed per amount of carbon (mg/g), k_2 (g/mg.st) is the pseudo-2nd-order rate constant, and t (h) is the contact time. By plotting t/qt versus t, 1/qe is obtained from the slope of the line and $1/(k_2.(qe)^2)$ is obtained from the intersection point [25].
The intraparticle diffusion model is expressed by Equation (5),

$$q_t = k_{id} t^{0.5} + C \quad (5)$$

where; intraparticle diffusion model rate constant is k_{id} ($mg/g.min^{0.5}$). By plotting qt versus $t^{1/2}$, the k_{id} value is found from the slope of the line obtained and the value of C is found from the intersection point.

5. Isotherms

Adsorption equilibrium isotherms give information about the adsorption mechanism. The relationship between adsorbent and adsorbed is described using isotherms [26, 27].
In this study, Langmuir and Freundlich's models were applied for adsorption data. The Langmuir equation describes a homogeneous and monolayer adsorption mechanism. The Freundlich equation, on the other hand, fits with a

heterogeneous surface and multilayer adsorption mechanism. In all isotherm calculasions, Ce (mg/L) is the Cr(VI) concentration at equilibrium and qe is the amount of adsorbed material at equilibrium (mg/g).
The Langmuir isotherm model is represented by the following equation [28].

$$\frac{C_e}{q_e} = \frac{1}{Q_o b} + \frac{C_e}{Q_o} \quad (6)$$

where, b (L/mg) is the Langmuir adsorption constant and Q_0 (mg/g) is the adsorption capacity. Figure 4 shows the Langmuir adsorption isotherm for Cr(VI) removal at different temperatures. The linear form of the Freundlich isotherm equation is represented by the following equation [28],

$$\ln(q_e) = \frac{1}{n}\ln(C_e) + \ln K_f \quad (7)$$

where, K_f (L/g) indicating the capacity constant of adsorption and n is the intensity constant of adsorption. Figure 6 shows the graphs of ln(Ce) versus ln(qe) at adsorption temperatures of 25, 35 and 45 ºC. K_f was calculated from the slope and n value was calculated from intercept of the ln(Ce) versus ln(qe) plot.

6. Thermodynamics

The (8), (9), and (10) equations were applied to determine the enthalpy (ΔH°), entropy (ΔS°) and free Gibbs energy (ΔG°) values.

$$\Delta G° = -RT \ln Kc \quad \text{and} \quad \Delta G° = \Delta H° - T\Delta S° \quad (8)$$

where, Kc is equilibrium constant, R is gas constant (8.314 Jmol/K) and T (K) is temperature. The Kc value was calculated from the following equation;

$$K_C = \frac{q_e}{C_e} \quad (9)$$

The ΔH° and ΔS° values can be calculated from the equation of Van't Hoff:

$$InK_C = \frac{\Delta S°}{R} - \frac{\Delta H°}{RT} \quad (10)$$

The ΔH° was calculated from the slope and ΔS° was calculated from the intercept of ln (K_c) plotted versus 1/T and the thermodynamic data are given in Table 5.

RESULTS AND DISCUSSIONS

1. Characterization

The surface characteristics obtained by N_2 adsorption on activated carbons which are produced at different impregnation ratios at 400 ºC carbonization temperature are given in Table 1.

Table 1. Surface characteristics of activated carbons.

Sample ID	S_{BET} (m^2/g)	V_{micro} (cm^3/g)	V_{meso} (cm^3/g)	V_{tot} (cm^3/g)	D_p (Å)
PL2-400	367.66	0.122	0.262	0.384	41.04
PL3-400	742.64	0.260	0.303	0.563	30.34
PL4-400	1345.26	0.456	0.482	0.938	27.91

H_3PO_4 has two important roles as an activation agent; the first is to ensure the degradation of precursor and the second is to ensure the formation of cross-linked structures [29]. In addition, H_3PO_4 provides the development of meso and micropores in activated carbon. The chemical impregnation ratio is also an significant factor for improving porosity in activated carbon production [30]. It is seen in Table 1 that as the impregnation ratio increases from 2 to 4, the specific surface area and total pore volume rise. Increasing the acid ratio encouraged the increase of

porosity in the structure. Similar results were found in wood-based activated carbons obtained with H_3PO_4 activation [22, 31]. The highest pore volume and surface area were observed with 4:1 H_3PO_4/poplar sawdust ratio of 0.938 cm^3/g and 1345.26 m^2/g, respectively. According to these results, all of the activated carbons produced at 400 °C at different acid ratios have micro and mesoporous structures. The N_2 isotherms and pore size distributions are given in Figure 1.

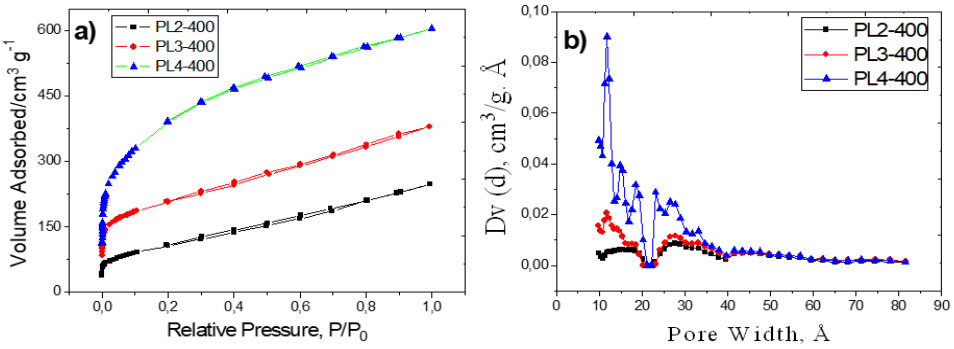

Figure 1. (a) N_2 isotherm and (b) pore-size distribution of PL(2, 3, 4)-400 activated carbons.

The N_2 isotherms given in Figure 1 (a) correspond to Type I and IV isotherm. In the activated carbons isotherms, the adsorption and desorption arms are almost coincident and the hysteresis region is very small but its presence is seen. This result indicates that activated carbon consist of meso and micropore structures. The pore size distribution plot in Figure 1 (b) shows a significant density in the size of up to 20 Å for all three activated carbons. The highest pore density was observed in PL4-400 at about 11.8 Å. This distribution up to 40 Å indicated that the activated carbons were composed of micro and meso pores. SBET surface area and isotherm curves also support this conclusion. It can be said that the impregnation rate in H_3PO_4 chemical activation is effective in improving the pore structure and surface area. In the SEM image of the activated carbons in Figure 2 (a), it is observed that the raw material has a flatter structure, while in Figures 2 (b), (c), and (d), it is clearly seen that the activated carbons with 2:1, 3:1 and 4:1 impregnation ratios, respectively, have a porous structure. The raw material structure was disrupted with H_3PO_4 activation and contributed to the formation of this porous structure. As the impregnation ratios increased, the pore volume of activated carbons increased. For this reason, the surface area also increased.

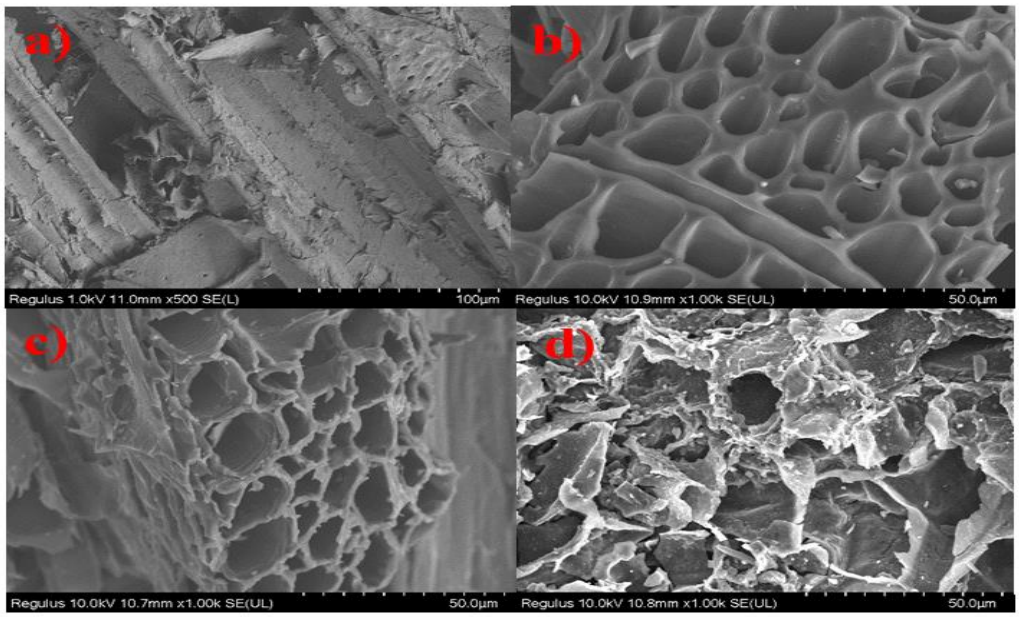

Figure 2. SEM images of (a) Poplar, (b) PL2-400, (c) PL3-400, and (d) PL4-400.

Table 2. EDX analysis results of activated carbons.

Samples	Element	Weight%
PL2-400	C	93.08
	N	0.14
	O	4.52
	P	2.26
PL3-400	C	87.89
	N	0.00
	O	4,58
	P	7.53
PL4-400	C	82,63
	N	0.94
	O	4.98
	P	11.45

As a result of EDX analysis, it was observed that the %C content of carbons decreased and %P content increased as the impregnation ratio increased. This result may be due to the degradation of some aliphatic and aromatic groups and their removal from the structure of the raw material as the amount of H_3PO_4 increases. PL4-400 activated carbon was determined to contain 82.63% carbon, 11.45% P, 4.98% O, and 0.94% N.

The functional groups of activated carbon and the poplar sawdust identify by FTIR analysis was performed. The spectrums are given in Figure 3. As a result of H_3PO_4 impregnation, the existing hydrogen bonds in the structure of the raw material are expected to be broken and different chemical bonds are expected to form. The chains separate and the structure expands. As the acid ratio increases, phosphate cross-links become bulkier to form polyphosphates. For this reason, the activated carbons' FTIR spectrum differ from the spectra of the raw material [32]. The weak bands between 500 and 600 cm^{-1} seen in the FTIR spectrum of PL4-400 activated carbon represent aromatic structures [31]. The 900-1000 cm^{-1} band is usually found on oxidized carbons and is attributed to CO stretching in single-bonded alcohols, acids, ethers or ester groups and phenols. However, it has also been reported to be characteristics of phosphorus and phospho-carbon compounds present in H_3PO_4-activated carbons. These bands were attributed to the P=OOH groups vibration or to the O-C stretching vibration [33]. In the PL4-400 spectrum, these structures were observed around 750-1000 cm^{-1}. The bands around 1500 cm^{-1} are identified as stretching of unsaturated C─C bonds for activated carbons obtained with H_3PO_4 activation or C═O band stretching that attributed to aromatic structures [31]. Bands between 1800-2450 cm^{-1} are attributed to the presence of esters, carboxylic acids, carbonyls, and aldehydes on the carbon surface [34]. The bands at 3900-3700 cm^{-1} are the O-H vibration and are usually attributed to hydrogen bonding in water [35].

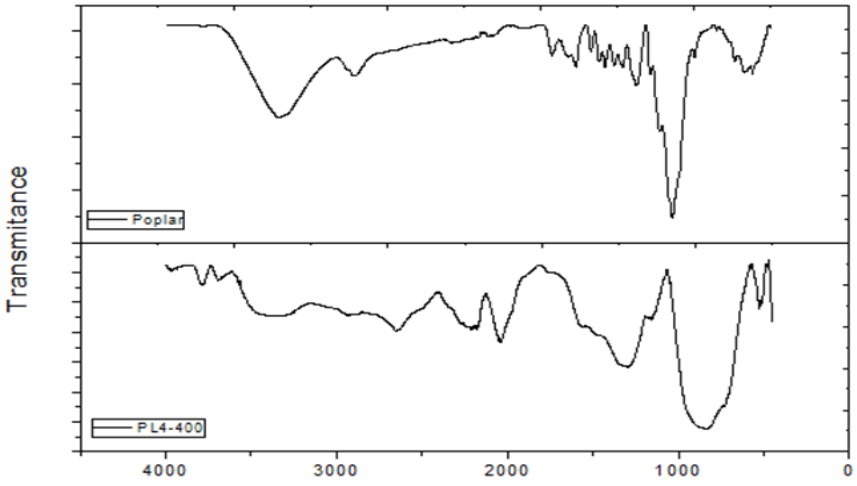

Figure 3. FTIR spectrum of Poplar and PL4-400.

2. Cr(VI) heavy metal adsorption

As PL4-400 activated carbon has the highest pore volume and surface area compared to the others, analyses were performed for the removal of Cr(VI) heavy metal. The pH effect on Cr(VI) adsorption was investigated with 0.05 g activated carbon for a 50 mg/L initial concentration at 25 °C for 24 hours at different pHs (2-5, 7, and 9). The graph showing the pH effect on adsorption is given in Figure 4a. While 100% removal was achieved at pH=2, the removal decreased with increasing pH values. The reason why the removal decreases as the pH value increases is that the chromium ions are in the form of H_2CrO_4 at pH=1.0. In the pH range of 1.0-6.0, chromium ions can coexist in the forms of $Cr_2O_7^-$, $HCrO_4^-$, Cr_3O10^{2-}, $Cr_4O_{13}^{2-}$, and the most dominant form is $HCrO_4^-$. When the pH value rises, this form shifts to CrO_4^{2-} and $Cr_2O_7^{2-}$. The stability of these different forms of chromium depends on the pH of the system. The balance between the different types of ionic chromium is as follows:

$$H_2CrO_4 \leftrightarrow H^+ + HCrO_4^- \quad (11)$$

$$HCrO_4^{2-} \leftrightarrow H^+ + CrO_4^{2-} \quad (12)$$

$$2HCrO_4^- \leftrightarrow Cr_2O_7^{2-} + H_2O \quad (13)$$

There is an rise in H^+ ions on the carbon surface at low pH values. Adsorption increases as a consequence of the electrostatic attraction between the positively charged surface and the chromate ions. Cr(VI) is predominantly in the form of $HCrO_4^-$ in the acidic pH range, and $HCrO_4^-$ ions have a greater affinity for H^+ ions on the activated carbon surface. For this reason, the removal decreased with increasing pH values. Similar results are found in the literature [36, 37]. Since the removal reached the maximum at pH=2, adsorption studies were continued at this pH value.

The effect of the amount of adsorbent was investigated with the amount of activated carbon varying between 0.001 and 0.1 g. Solutions at the original pH value in 50 ml volume with a 50 mg/L initial concentration were kept in a shaking water bath at 25 °C for 24 h. The graphs of the results obtained are given in Figure 4b. With the rise in the adsorbent amount, the adsorption capacity increased; the highest removal was obtained with 0.1 g activated carbon at 81.62%.

Since it was observed that the adsorption yield increased with the effect of pH, the equilibrium time was investigated by taking samples at a 50 mg/L initial concentration with 0.05 g activated carbon at pH=2, at 25 °C, in the range of 0-20 h. The graph of the results obtained is given in Figure 4c. Under these conditions, the adsorption reached equilibrium in 16 h. In order to shorten the equilibrium time, the studies were repeated under the same conditions with 0.1 g of activated carbon between 0-8 h and in 6 h adsorption was reached the equilibrium.

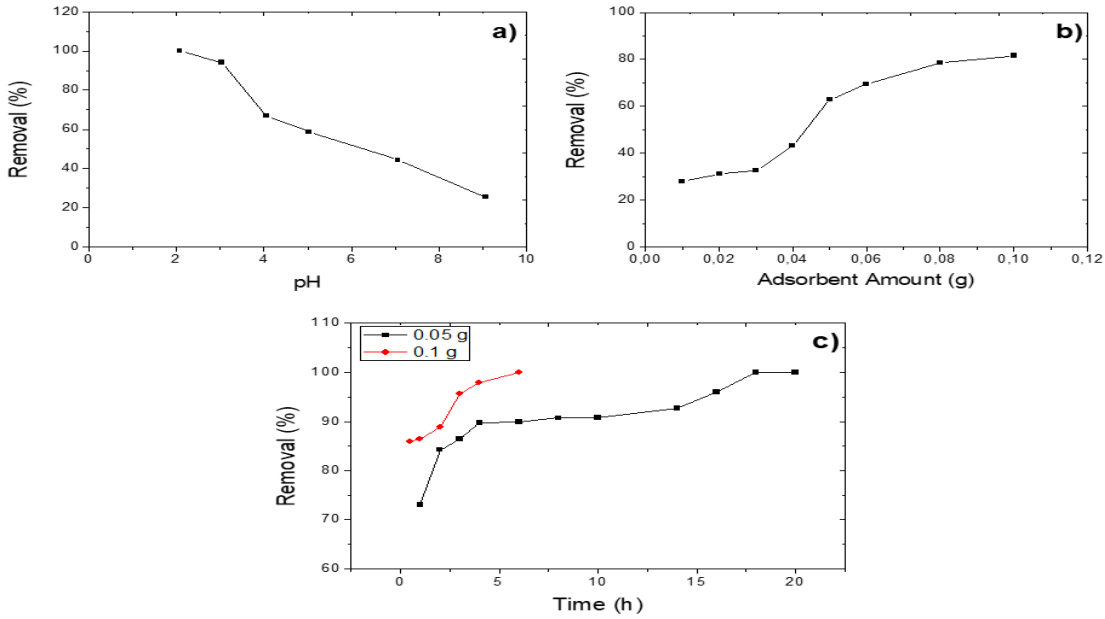

Figure 4. Analysis of the Cr(VI) heavy metal: (a) the effect of pH on the amount of adsorbed substance, (b) the effect of the amount of adsorbent on adsorption, and (c) the change of the amount of adsorbed material over time.

Pseudo-1st and pseudo-2nd kinetic order models were applied to the kinetic data to determine the order and rate constant. Theoretical q_e values were calculated according to the graphs drawn for both models. These results are given in Figure 5 and the kinetic parameters for the rate expressions are given in Table 3. According to the results obtained, the theoretical q_e calculated for the 2nd-degree kinetic model is quite close to the experimental q_e value. In addition, the R^2 coefficient of the 1st-order model is lower than the kinetic 2nd-order kinetic model. These results indicate that the pseudo-2nd order mechanism is dominant in Cr(VI) adsorption mechanism. Similar outputs were found in Cr(VI) adsorption studies with different activated carbons [38, 39].

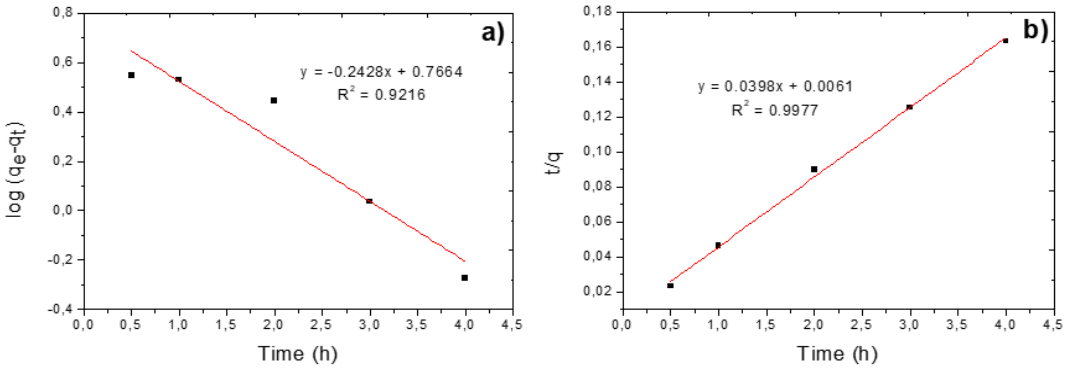

Figure 5. Adsorption kinetics for pseudo-I and II-order rate equations.

Table 3. Kinetic parameters of PL4-400.

q_e *(mg/g)*	*Pseudo I*			*Pseudo II*		
(Experimental)	k_1 (1/st)	q_e (mg/g)	R^2	k_2 (g/mg.st)	q_e (mg/g)	R^2
25.00	0.559	5.840	0.9216	0.259	25.126	0.9977

The variation of the adsorption capacity depending on the initial concentration and temperature is given in Figure 6. As seen in Figure 6, it is observed that the adsorption capacity increases with rising temperature for the same initial concentrations. The highest adsorption capacity (117.15 mg/g) was obtained at 45 °C for an initial concentration of 250 mg/L. The increase in adsorption efficiency with increasing temperature can be explained by the low kinetic energy of $Cr_2O_7^{2-}$ anions at low temperatures, and therefore the insufficient contact with the active sites in the structure of activated carbons [40]. In addition, the % removal decreased with increasing initial concentrations. At 50-250 mg/L initial concentrations range, % Cr(VI) removal had changed from 96.56% to 85.34% for 25 °C, from 100% to 90.55% for 35 °C, and from 100% to 93.72% for 45 °C. This can be described by the fact that activated carbons have a limited active sites number that become saturated after a certain concentration. The removal yield decreases as the active adsorption sites of the activated carbon will be saturated at a high initial concentration [40, 41].

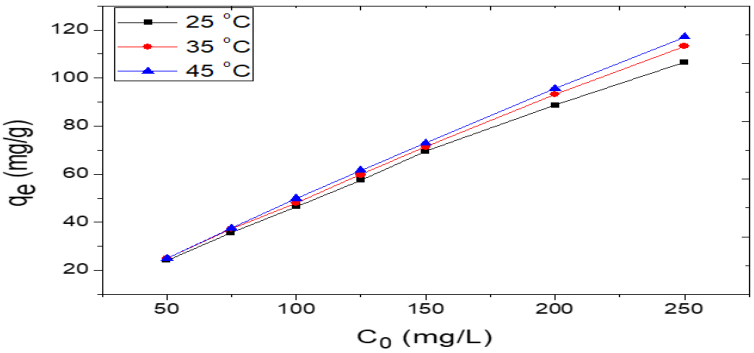

Figure 6. The initial concentration effect at different temperatures.

Langmuir constants Q_0 and b were calculated according to Eq. 6 by plotting C_e vs. C_e/q_e values for 3 different temperature values. Calculated correlation coefficients and Langmuir constants are given in Table 4. The high R^2 coefficients obtained show that the adsorption of Cr(VI) with activated carbon is compatible with the Langmuir model. For Cr(VI) adsorption on activated carbon, the adsorption constants and correlation coefficients calculated from Equation 7 with the Freundlich adsorption isotherm drawn according to the adsorption data obtained at different initial concentrations and different temperatures at pH=2 are given in Table 4. The R^2 coefficients obtained from the graphs drawn according to both isotherm models at varied temperatures are similar, and the R^2 coefficient of the Langmuir isotherm are higher at 25 °C and 45 °C temperatures. Freundlich constants K_f is the indicate the adsorption capacity of the adsorbent and n value is the availability of adsorption. The highest K_f value was obtained at 45 °C. The 1/n values are less than 1, indicating that Cr(VI) adsorption on activated carbon is more compatible with the Langmuir adsorption model.

Table 4. Isotherm constants for adsorption of Cr(VI) on PL4-400.

	Temperature (ºC)	*R^2*	*Q_0 (mg/g)*	*b (L/mg)*
Langmuir	25	0.973	135.135	0.090
	35	0.912	120.482	0.313
	45	0.991	113.636	1.173
	Temperature (°C)	*R^2*	*1/n*	*K_f*
Freundlich	25	0.949	0.484	19.364
	35	0.986	0.491	25.598
	45	0.939	0.169	61.944

The adsorption of Cr(VI) on PL4-400 confirmed to the Langmuir model. The natural logarithm of Langmuir's constant b versus 1/T was plotted, and ΔH° from its slope and ΔS° from its cutoff point, then ΔG° was calculated by substituting these values in Equation 8. The results obtained are given in Table 5. Since ΔG° was negative and ΔH° and ΔS° were positive, adsorption was spontaneous and endothermic. The negative ΔG° value indicates that the adsorption process is spontaneous, while the ΔG° value decreases at higher temperatures. The positive value of ΔH° indicates that adsorption is an endothermic process.
The positive ΔS° value indicates increased disorder at the solid-solution interface and the affinity of the adsorbent molecules for Cr(VI). The Cr(VI) amount that adsorbed with increasing temperature also confirms this result. Yang et al [39] and Acharya et al [42] obtained similar results in their studies

Table 5. Thermodynamic expressions for Cr(VI) adsorption on PL4-400

ΔH(kJ mol^{-1})	*ΔS(kJ mol^{-1} K^{-1})*	*ΔG (kj /mol K)*		
16.096	0.0604	25 ºC	35 ºC	45 ºC
		-1.900	-2.504	-3.107

CONCLUSIONS

- It is possible to develop economical adsorbents to remove Cr(VI) from aqueous solutions. Synthesis of activated carbon from biomass (poplar sawdust) is important in terms of both low cost and recycling. This research shows that the poplar sawdust based activated carbon is an efficient adsorbent for the Cr(VI) adsorption. The outputs of the study are;
- The BET analysis results showed that PL4-400 had a 1345.26 m^2/g specific surface area and a 0.938 cm^3/g pore volume.
- It was observed in SEM-EDX analyses that as the amount of H_3PO_4 increased, the %C content of carbons decreased and the %P content increased due to the degradation of some aliphatic and aromatic groups and removal of the raw material from its structure.

- The Cr(VI) adsorption on PL4-400 was performed with different pH values. Since there is an increase in H^+ ions on the surface at low pH values, adsorption increases as a result of the electrostatic attraction between the chromate ions and the positively charged surface. According to the results obtained with different adsorbents, the adsorption capacity rised with the increased amount of adsorbent.
- Adsorption kinetics of Cr(VI) removal on PL4-400 activated carbon were obtained according to pseudo-1st order and 2nd order. It showed that the pseudo-2nd-order adsorption mechanism was dominant in the Cr(VI) adsorption mechanism.
- The relationship between adsorbent and adsorbed was described using the isotherms of Langmuir and Freundlich. The high correlation coefficients obtained showed that the adsorption of Cr(VI) with activated carbon is compatible with the Langmuir model compared to the Freundlich model.
- $\Delta H°$, $\Delta S°$, and $\Delta G°$ values were calculated by making thermodynamic calculations. Since $\Delta G°$ was negative, $\Delta H°$ and $\Delta S°$ were positive, it was concluded that adsorption is spontaneous and endothermic.
- In light of the results obtained, it has been shown that activated carbon obtained from poplar sawdust can be effectively used as an adsorbent for Cr(VI) removal.

Declarations. **Ethical Approval:** No animal or human experimental studies have been conducted in this manuscript. **Competing Interests:**There is no financial or personal conflict of interest in the obtained work. **Authors' Contributions:** İzge Demir: Methodology/study design, visualization; Aykut Caglar: Writing – review and editing, resources; Derya Yildiz: Supervision, investigation, project administration; **Funding:** not applicable **Availability of data and materials:** not applicable

REFERENCES

1. P. Chowdhury, S. Athapaththu, A. Elkamel, A.K. Ray, Visible-solar-light-driven photo-reduction and removal of cadmium ion with Eosin Y-sensitized TiO2 in aqueous solution of triethanolamine, Separation and Purification Technology, 174 (2017) 109-115;
2. M.D. Esteban-Vasallo, N. Aragones, M. Pollan, G. López-Abente, B. Perez-Gomez, Mercury, cadmium, and lead levels in human placenta: a systematic review, Environ. Health Perspect., 120 (2012) 1369-1377;
3. G. Aragay, J. Pons, A. Merkoçi, Recent trends in macro-, micro-, and nanomaterial-based tools and strategies for heavy-metal detection, Chem. Rev., 111 (2011) 3433-3458;
4. Ş. Yılmaz, A. Zengin, Y. Akbulut, T. Şahan, Magnetic nanoparticles coated with aminated polymer brush as a novel material for effective removal of Pb (II) ions from aqueous environments, Environmental Science and Pollution Research, 26 (2019) 20454-20468;
5. P. BELİBAĞLI, B.N. ÇİFTCİ, Y.U. UYSAL, Chromium (Cr (VI)) removal from water with bentonite-magnetite nanocomposite using response surface methodology (RSM), Sigma Journal of Engineering and Natural Sciences, 38 (2020) 1217-1233;
6. C. Zamora-Ledezma, D. Negrete-Bolagay, F. Figueroa, E. Zamora-Ledezma, M. Ni, F. Alexis, V.H. Guerrero, Heavy metal water pollution: A fresh look about hazards, novel and conventional remediation methods, Environmental Technology & Innovation, 22 (2021) 101504;
7. Y. Kojima, Y.J. Machida, DNA–protein crosslinks from environmental exposure: mechanisms of formation and repair, Environ. Mol. Mutagen., 61 (2020) 716-729;
8. D. Lapworth, A. MacDonald, S. Kebede, M. Owor, G. Chavula, H. Fallas, P. Wilson, J. Ward, M. Lark, J. Okullo, Drinking water quality from rural handpump-boreholes in Africa, Environmental Research Letters, 15 (2020) 064020;
9. R.A. Alfadaly, A. Elsayed, R.Y.A. Hassan, A. Noureldeen, H. Darwish, A.S. Gebreil, Microbial Sensing and Removal of Heavy Metals: Bioelectrochemical Detection and Removal of Chromium(VI) and Cadmium(II), Molecules, 26 (2021) 2549;
10. X. Sun, H. Huang, Y. Zhu, Y. Du, L. Yao, X. Jiang, P. Gao, Adsorption of Pb2+ and Cd2+ onto Spirulina platensis harvested by polyacrylamide in single and binary solution systems, Colloids and Surfaces A: Physicochemical and Engineering Aspects, 583 (2019) 123926;
11. K. Kalantari, M.B. Ahmad, H.R.F. Masoumi, K. Shameli, M. Basri, R. Khandanlou, Rapid and high capacity adsorption of heavy metals by Fe3O4/montmorillonite nanocomposite using response surface

methodology: preparation, characterization, optimization, equilibrium isotherms, and adsorption kinetics study, Journal of the Taiwan institute of Chemical Engineers, 49 (2015) 192-198;
12. T. Song, C. Yu, X. He, J. Lin, Z. Liu, X. Yang, Y. Zhang, Y. Huang, C. Tang, Synthesis of magnetically separable porous BN microrods@ Fe3O4 nanocomposites for Pb (II) adsorption, Colloids and Surfaces A: Physicochemical and Engineering Aspects, 537 (2018) 508-515;
13. G. Feng, J. Ma, X. Zhang, Q. Zhang, Y. Xiao, Q. Ma, S. Wang, Magnetic natural composite Fe3O4-chitosan@bentonite for removal of heavy metals from acid mine drainage, J. Colloid Interface Sci., 538 (2019) 132-141;
14. S.S. Fiyadh, M.A. AlSaadi, W.Z. Jaafar, M.K. AlOmar, S.S. Fayaed, N.S. Mohd, L.S. Hin, A. El-Shafie, Review on heavy metal adsorption processes by carbon nanotubes, Journal of Cleaner Production, 230 (2019) 783-793;
15. P.S. Kwon, R. Shahrokhi, J. Park, H. Kim, Zeolite mixtures as adsorptive fill material with sustainable bearing capacity, Waste Management and the Environment IX, 20 (2019) 91;
16. M. Li, S.A. Messele, Y. Boluk, M.G. El-Din, Isolated cellulose nanofibers for Cu (II) and Zn (II) removal: performance and mechanisms, Carbohydrate polymers, 221 (2019) 231-241;
17. D. Eeshwarasinghe, P. Loganathan, S. Vigneswaran, Simultaneous removal of polycyclic aromatic hydrocarbons and heavy metals from water using granular activated carbon, Chemosphere, 223 (2019) 616-627;
18. J. Salimi, B. Kakavandi, A.A. Babaei, A. Takdastan, N. Alavi, A. Neisi, B. Ayoubi-Feiz, Modeling and optimization of nonylphenol removal from contaminated water media using a magnetic recoverable composite by artificial neural networks, Water Sci. Technol., 75 (2017) 1761-1775;
19. R. Shahrokhi-Shahraki, C. Benally, M.G. El-Din, J. Park, High efficiency removal of heavy metals using tire-derived activated carbon vs commercial activated carbon: Insights into the adsorption mechanisms, Chemosphere, 264 (2021) 128455;
20. L. Li, D. Zou, Z. Xiao, X. Zeng, L. Zhang, L. Jiang, A. Wang, D. Ge, G. Zhang, F. Liu, Biochar as a sorbent for emerging contaminants enables improvements in waste management and sustainable resource use, Journal of Cleaner Production, 210 (2019) 1324-1342;
21. R. Shahrokhi-Shahraki, P.S. Kwon, J. Park, B.C. O'Kelly, S. Rezania, BTEX and heavy metals removal using pulverized waste tires in engineered fill materials, Chemosphere, 242 (2020) 125281;
22. C. Saka, D. Yıldız, S. Kaya, A. Caglar, D. Elitok, E. Yaylı, M. Kaya, R. Atelge, H. Kivrak, A novel hazelnutt bagasse based activated carbon as sodium borohydride methanolysis and electrooxidation catalyst, International Journal of Hydrogen Energy, (2023);
23. F. Ghorbani, S. Kamari, S. Zamani, S. Akbari, M. Salehi, Optimization and modeling of aqueous Cr(VI) adsorption onto activated carbon prepared from sugar beet bagasse agricultural waste by application of response surface methodology, Surfaces and Interfaces, 18 (2020) 100444;
24. S. Kaya, C. Saka, D. Yildiz, S. Erol, B. Ulas, I. Demir, H. Kivrak, Enhanced hydrogen production via methanolysis and energy storage on novel poplar sawdust-based biomass-derived activated carbon catalyst, Journal of Applied Electrochemistry, (2023);
25. E. Demirbas, N. Dizge, M.T. Sulak, M. Kobya, Adsorption kinetics and equilibrium of copper from aqueous solutions using hazelnut shell activated carbon, Chemical Engineering Journal, 148 (2009) 480-487;
26. E. Menya, P.W. Olupot, H. Storz, M. Lubwama, Y. Kiros, Production and performance of activated carbon from rice husks for removal of natural organic matter from water: A review, Chemical Engineering Research and Design, 129 (2018) 271-296;
27. S. Sinha Ray, R. Gusain, N. Kumar, Adsorption equilibrium isotherms, kinetics and thermodynamics, in, 2020, pp. 101-118;
28. U. Selengil, D. Yildiz, Investigation of the methylene blue adsorption onto waste perlite, Desalination and Water TREATMENT, 262 (2022) 235-247;
29. T. Budinova, E. Ekinci, F. Yardim, A. Grimm, E. Björnbom, V. Minkova, M. Goranova, Characterization and application of activated carbon produced by H3PO4 and water vapor activation, Fuel processing technology, 87 (2006) 899-905;
30. D. Prahas, Y. Kartika, N. Indraswati, S. Ismadji, Activated carbon from jackfruit peel waste by H3PO4 chemical activation: Pore structure and surface chemistry characterization, Chemical Engineering Journal, 140 (2008) 32-42;

31. S. Yorgun, D. Yıldız, Preparation and characterization of activated carbons from Paulownia wood by chemical activation with H3PO4, Journal of the Taiwan Institute of Chemical Engineers, 53 (2015) 122-131;
32. M. Jagtoyen, F. Derbyshire, Activated carbons from yellow poplar and white oak by H3PO4 activation, Carbon, 36 (1998) 1085-1097;
33. J. Xu, L. Chen, H. Qu, Y. Jiao, J. Xie, G. Xing, Preparation and characterization of activated carbon from reedy grass leaves by chemical activation with H3PO4, Applied Surface Science, 320 (2014) 674-680;
34. M. Rai, G. Shahi, V. Meena, R. Meena, S. Chakraborty, R. Singh, B. Rai, Removal of hexavalent chromium Cr (VI) using activated carbon prepared from mango kernel activated with H3PO4, Resource-efficient technologies, 2 (2016) S63-S70;
35. H.S. Karapınar, Adsorption performance of activated carbon synthesis by ZnCl2, KOH, H3PO4 with different activation temperatures from mixed fruit seeds, Environ. Technol., 43 (2022) 1417-1435;
36. H. Haroon, J.A. Shah, M.S. Khan, T. Alam, R. Khan, S.A. Asad, M.A. Ali, G. Farooq, M. Iqbal, M. Bilal, Activated carbon from a specific plant precursor biomass for hazardous Cr (VI) adsorption and recovery studies in batch and column reactors: Isotherm and kinetic modeling, Journal of Water Process Engineering, 38 (2020) 101577;
37. T. Karthikeyan, S. Rajgopal, L.R. Miranda, Chromium (VI) adsorption from aqueous solution by Hevea Brasilinesis sawdust activated carbon, J. Hazard. Mater., 124 (2005) 192-199;
38. A.K. Giri, R. Patel, S. Mandal, Removal of Cr (VI) from aqueous solution by Eichhornia crassipes root biomass-derived activated carbon, Chemical Engineering Journal, 185 (2012) 71-81;
39. J. Yang, M. Yu, W. Chen, Adsorption of hexavalent chromium from aqueous solution by activated carbon prepared from longan seed: Kinetics, equilibrium and thermodynamics, Journal of industrial and engineering chemistry, 21 (2015) 414-422;
40. S. Mor, K. Ravindra, N. Bishnoi, Adsorption of chromium from aqueous solution by activated alumina and activated charcoal, Bioresource Technology, 98 (2007) 954-957;
41. J. Zhao, L. Yu, H. Ma, F. Zhou, K. Yang, G. Wu, Corn stalk-based activated carbon synthesized by a novel activation method for high-performance adsorption of hexavalent chromium in aqueous solutions, J. Colloid Interface Sci., 578 (2020) 650-659;
42. J. Acharya, J. Sahu, B. Sahoo, C. Mohanty, B. Meikap, Removal of chromium (VI) from wastewater by activated carbon developed from Tamarind wood activated with zinc chloride, Chemical Engineering Journal, 150 (2009) 25-39;